Renewable Energy 237 (2024) 121668

Contents lists available at ScienceDirect

Renewable Energy

journal homepage: www.elsevier.com/locate/renene

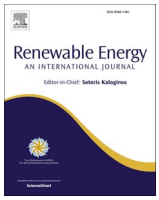

Development and characterization of mesoporous silica-$MgSO_4$-$MgCl_2$ binary salt composites for low-grade heat storage in fluidized bed systems

Xiao Liu [a], Fangming Yang [a,**], Xin Liu [a,b], Haomin Wang [a], Yupeng Wu [a,*]

[a] Faculty of Engineering, University of Nottingham, Nottingham, NG7 2RD, United Kingdom
[b] University of Lincoln, Brayford Pool, Lincoln, LN6 7TS, United Kingdom

ARTICLE INFO

Keywords:
Binary-salt composite
Fluidization
Hydration
Agglomeration
Temperature lift
Energy storage density (ESD)

ABSTRACT

Achieving nearly zero-energy buildings requires the efficient utilization and storage of renewable energy. Salt-hydrate-based thermochemical energy storage (TCES) systems are promising due to their high heat storage capacity and minimal seasonal heat loss. However, challenges remain in their commercialization and large-scale application. For instance, TCES systems using magnesium sulphate ($MgSO_4$) provide low temperature lifts due to slow reaction kinetics. Incorporating deliquescent salts like magnesium chloride ($MgCl_2$) can enhance sorption performance but may introduce stability issues such as agglomeration and decomposition. This study presents a novel binary-salt composite combining $MgSO_4$ and $MgCl_2$ within commercial mesoporous silica (CMS) to address these challenges and enhance overall performance. The binary-salt composite powder, with a particle size range of 150–300 μm, is well-suited for use in fluidized-bed reactors, where fast mass and heat transfer promote efficient moisture adsorption, prevent uneven temperature distribution, and reduce agglomeration. Thermogravimetric analysis (TGA) was employed to evaluate the water sorption and desorption behaviour of $MgCl_2$-$MgSO_4$@CMS binary-salt composites with a total salt content of 50 wt% and salt mixing ratios of 3:1, 1:1, and 1:3. The corresponding water sorption capacities were 0.95, 0.68, and 0.57 g/g, respectively. In comparison, the $MgSO_4$@CMS single-salt composite showed a lower water adsorption capacity of 0.47 g/g and required temperatures exceeding 150 °C for complete regeneration. Reactor-scale experiments demonstrated that the $MgCl_2$-$MgSO_4$@CMS composite with a 1:1 salt mixing ratio could be fluidized at low gas velocities on the order of 10^{-2} m/s, achieving a maximum temperature lift of 24.7 °C and an energy density of 1018 kJ/kg during hydration at 80% relative humidity and 30 °C. Additionally, the binary-salt composite showed good cyclic stability with less particle agglomeration compared to the $MgCl_2$@CMS single-salt composite.

1. Introduction

In the fight against climate change, thermal energy storage (TES) is a crucial technology that stores renewable energy for later use, ensuring a consistent energy supply and supporting the transition toward carbon neutrality. TES materials are classified into three categories: sensible heat storage (SHS), latent heat storage (LHS) and thermochemical energy storage (TCES). Thermochemical materials are notable for their high energy density and minimal heat loss, which allow for the design of compact systems and enable long-term or seasonal storage. TCES achieves these benefits through reversible sorption/desorption processes or chemical reactions, where compounds decompose and recombine to store and release heat. TCES systems can be used across a broad range of scales, from small domestic systems to large industrial installations. They can be integrated with various energy conversion technologies such as solar collectors [1], heat pumps [2], air conditioning units [3], Trombe wall [4], and concentrating solar power (CSP) systems [5].

While TCES systems are still in early development, certain working pairs have shown suitability for building applications. Examples include lithium bromide salt solution (absorbent)/H_2O (sorbate) and zeolite (adsorbent)/H_2O (sorbate), with the former successfully applied in commercial absorption chillers and heat pumps [6,7], and the latter widely used in conventional packed-bed reactors for domestic air or water heating [8–10]. Composites 'salt in porous matrix' (CSPMs) are recognized as a promising class of sorption materials for the development of building-scale TCES systems. Compared to zeolites, CSPMs can

* Corresponding author.
** Corresponding author.
E-mail addresses: fangming.yang@nottingham.ac.uk (F. Yang), yupeng.wu@nottingham.ac.uk (Y. Wu).

https://doi.org/10.1016/j.renene.2024.121668
Received 5 September 2024; Received in revised form 14 October 2024; Accepted 21 October 2024
Available online 22 October 2024

be regenerated at lower temperatures (80–150 °C), possess higher energy density, and cost less when loaded with inexpensive salt hydrates [11,12]. In contrast to pure salts, CSPMs experience less agglomeration and smaller volume change, though they tend to have a lower water sorption capacity due to the partial substitution of salts with inactive substances [13]. Despite these advantages, the commercialization and widespread adoption of CSPMs still face challenges related to heat storage capacity, reaction kinetics, scalability, and system integration.

The key to unlocking the full potential of CSPMs lies in the careful selection of the host matrix and impregnated salts. Different porous materials, with their distinct morphologies and structural properties—including pore size distribution, pore volume, and surface area—can significantly affect the water sorption performance of CSPMs [14–16]. For instance, using matrices with larger pore sizes and pore volumes enables greater salt loading capacity and higher water uptake [17], while those with interconnected porous structures or larger surface areas allow for faster water vapour diffusion, resulting in improved de/sorption kinetics [18–20]. Additionally, the choice of impregnated salts is crucial, as it determines the charging and discharging temperatures, as well as the heat storage capacity of CSPMs. An example is the incorporation of deliquescent salts, such as magnesium chloride ($MgCl_2$), into zeolites to achieve multi-form sorption processes, including physical adsorption, chemical adsorption and liquid absorption. This method achieves a higher energy density (1368 kJ/kg) compared to pure zeolites (291–784 kJ/kg) [21–24] and magnesium sulphate ($MgSO_4$)@zeolite (407–721 kJ/kg) [22,23,25,26]. Ousaleh et al. [27] used a blend of bentonite clay and expanded graphite as the host matrix for impregnating deliquescent salts, such as lithium chloride (LiCl), strontium chloride ($SrCl_2$) and calcium chloride ($CaCl_2$), achieving energy densities of 704.2, 854.5 and 778.6 kJ/kg, respectively.

Factors such as particle size, particle shaping technique, thermal conductivity, and bulk density also play crucial roles in the performance of composite materials. Brancato et al. [28] prepared LiCl@vermiculite composites and observed slower water sorption kinetics when the particle size was increased from 1.7–2.0 mm to 2.36–2.80 mm. Touloumet et al. [29] noted reductions in the micropore volume and specific surface area of zeolites when a binder was used. They found that binderless zeolite powder exhibited faster and greater water sorption (0.31 g/g) than zeolites beads with a binder (0.28 g/g). Similarly, $CaCl_2$@zeolite composite in powder form showed higher water sorption (0.29 g/g) compared to its bead form (0.21 g/g). Miao et al. [30] impregnated $MgSO_4$ in expanded graphite, which improved the thermal conductivity by 84% and shortened the hydration time to one-fourth of its pure form. Gaeini et al. [31] prepared three CSPMs by impregnating $CaCl_2$ into vermiculite and expanded graphite, and by encapsulating it with ethyl cellulose. Despite its higher stability and reaction kinetics, the encapsulated $CaCl_2$ exhibited a lower volumetric energy density (0.4 GJ/m^3) compared to the impregnated materials (1.2 GJ/m^3) due to its lower bulk density.

The development of mixed salt (binary-salt or multi-salt) composite materials is an important direction for advancing CSPMs in TCES applications. Binary-salt composites, which integrate two distinct salts within a carrier material, can synergize their respective advantages and potentially offer better performance compared to single-salt composites [13]. For example, adding hydrothermally stable salts with high deliquescence relative humidity, such as $MgSO_4$ (DRH = 90% at 30 °C), to deliquescent salts like $MgCl_2$ (DRH = 33% at 30 °C) can mitigate aggregation and corrosion [32]. While $MgSO_4$ has poor re-hydration ability and slow kinetics, these drawbacks can be offset by the high kinetics of $MgCl_2$ [13]. Additionally, since $MgSO_4$ can partly dissolve in the $MgCl_2$ solution, higher $MgSO_4$ hydrates are more easily formed compared to pure $MgSO_4$ under similar humidity conditions [13]. This was validated in the study by Rammelberg et al. [13], where a mixture of $MgCl_2$ and $MgSO_4$ exhibited higher sorption capacity and faster kinetics than pure $MgSO_4$.

Posern and Kaps [32] impregnated attapulgite granulate with mixtures of $MgSO_4$ and $MgCl_2$ at various weight ratios. The heat of sorption increased with a higher proportion of $MgCl_2$, reaching 1590 kJ/kg at an $MgCl_2$/$MgSO_4$ mass ratio of 80:20. However, further studies including cyclic tests are needed to confirm the material stability. Zbair et al. [33] developed a composite consisting of binary salts (48 wt% $MgSO_4$ + 12 wt% $MgCl_2$) in porous carbon, achieving an energy density of 1840 kJ/kg, which represents 70% of the heat released by pure mixed salts. Comparatively, the mono-salt (60 wt% $MgSO_4$) composite possessed a lower energy density, 1356 kJ/kg, which is 52% of the heat liberated by pure $MgSO_4$. The use of binary salt hydrates also enhances resistance to corrosion, particularly when employing copper heat exchangers in contact with salts such as $MgCl_2$ and $CaCl_2$ [34]. Ousaleh et al. [35] measured the corrosion rates of copper metal immersed in a $MgCl_2$ solution as 50.38 mg cm^{-2} y^{-1} at 20 °C and 306.68 mg cm^{-2} y^{-1} at 80 °C. These values decreased by 59% and 62%, respectively, when using a $MgCl_2$-$MgSO_4$ mixture.

Binary salt hydrates can also be formulated using various chloride and/or sulphate based salts, such as LiCl-$MgSO_4$ [36,37], $SrCl_2$-$MgSO_4$ [38], $CaCl_2$-$MgSO_4$ [37,39], $MgCl_2$-zinc sulphate ($ZnSO_4$) [40], $MgSO_4$-$ZnSO_4$ [41], $MgCl_2$-$CaCl_2$ [13, 42], $MgCl_2$-potassium chloride (KCl) [43], and LiCl-$CaCl_2$ [44]. A few studies proposed ternary-salt composites, such as impregnating vermiculite with a $MgCl_2$-$MgSO_4$--lithium nitrate ($LiNO_3$) mixture [37]. Nevertheless, the inclusion of an additional salt may introduce compatibility issues with the other two salts, potentially leading to undesirable chemical reactions or reduced performance. Additionally, ternary-salt composites may require a more complex fabrication process and can complicate optimization efforts, such as determining the optimal salt mixing ratio.

In the literature, most previous studies focused on evaluating binary-salt composite particles at the material level, with some extending their analyses to the reactor scale. These studies typically employed open-type systems consisting of packed-bed reactors and air conditioning accessories (e.g., humidifier, electric heater, and airflow controller) to achieve hydration (heat discharging) and dehydration (heat charging) processes [37,42,45]. In a fixed-bed (also called packed-bed) reactor, particles exchange heat and moisture with the surrounding air, and the reaction rate is directly linked to the local temperature and humidity levels. These factors are determined by various elements such as reactor geometry [46], gas diffuser design [45,47], gas velocity [8], reactive bed thickness [48], particle shape and size [49], porosity [47], and material thermal conductivity [50]. A common drawback of fixed-bed reactors is the uneven distribution of heat and moisture [51]. This may cause CSPM particles to aggregate due to overhydration and prevent them from being restored to their anhydrous state due to insufficient charging temperatures. Alternative approaches, such as utilization of fluidized-bed reactors, hold promise for overcoming these limitations, but has not been extensively studied in the field of low-temperature TCES. Only a few studies have demonstrated prototypes and tests using fluidized-bed reactors with zeolite 13X [52] and $MgCl_2$@LiX zeolite [53]. However, the practicality of these systems is limited by the intrinsic drawbacks of zeolites, such as high charging temperatures (above 180 °C) and low salt loading capacity (typically below 15 wt% to avoid severe pore blockage).

The integration of TCES systems within buildings requires an optimized system design, including careful selection of storage materials, reactors, and system operating conditions. CSPMs are promising candidates due to their effectiveness in reducing agglomeration, swelling, and corrosion associated with pure salts. Using CSPMs with higher energy density is advantageous for designing a more compact system. The energy density of a single- or binary-salt composite can be improved by exposing it to higher humidity levels or by using a higher salt content. However, both methods may compromise material stability and increase the risk of liquid leakage. Previous studies on hydrating binary-salt composites generally employed partial water vapour pressures below 30 mbar, equivalent to a relative humidity (RH) of 70% at 30 °C or 95%

at 25 °C [13,33,36–38]. The salt content for impregnation in traditional porous matrices like zeolite [15,23,29] and silica gel [17,54], generally ranges from 5 to 20 wt%. Other factors, such as reactor type and particle size, can also influence the energy density and stability of CSPMs. Packed bed reactors with CSPM granules, pellets, or beads larger than 1 mm in diameter are commonly used due to their high energy density and simplicity. For submillimeter-size CSPMs powders, fluidized bed reactors is a viable choice, as they can promote powder-gas mixing, achieving faster heat/mass transfer and lower pressure drops compared to densely packed powder reactors. Nevertheless, there is limited literature about CSPM-based fluidized bed systems, and the feasibility of improving material performance by using high salt content and exposing the material to high humidity in fluidized beds has not yet been thoroughly investigated.

This study introduces a novel binary-salt composite consisting of mesoporous silica impregnated with a $MgSO_4$-$MgCl_2$ mixture, specifically designed for use in fluidized-bed reactors for low-grade heat storage. Traditional micro-porous matrices, such as zeolite 13X, are characterized by large specific surface areas but limited pore volumes (0.33–0.37 cm^3/g [29]). Conversely, marco-porous materials like expanded vermiculite offer large pore volumes but have low specific surface areas (5.6 m^2/g [28]). In contrast, the mesoporous silica combines both a large pore volume (1.79 cm^3/g) and a high specific surface area (283 m^2/g), allowing for a salt loading capacity of up to 50 wt% while maintaining rapid reaction kinetics. The impregnation of $MgCl_2$ and $MgSO_4$ allows the composite to operate stably under high partial water vapour pressures (up to 34 mbar) while achieving a high energy density (exceeding 1000 kJ/kg). Furthermore, the composite material can be fully regenerated using low-grade heat sources (120–150 °C), making it suitable for integration with solar thermal systems and waste heat recovery systems in buildings. Additionally, the composite powders can be easily fluidized at low gas velocities on the order of 10^{-2} m/s due to their appropriate particle sizes (150–300 μm).

To validate the concept, a binary-salt composite ($MgSO_4$-$MgCl_2$@CMS) and two single-salt composites ($MgSO_4$@CMS and $MgCl_2$@CMS), each with a total salt content of 50 wt%, were developed. Initial evaluations were conducted using thermogravimetric analysis (TGA), followed by tests in a lab-scale TCES system to assess fluidization quality, water sorption capacity, temperature lift, energy density, and cyclic stability. The performance of the $MgSO_4$-$MgCl_2$@CMS composite was studied under varying system operating conditions, including different hydration temperatures, relative humidities, partial water vapour pressures, and flow rates, and compared to another type of binary-salt composite, magnesium bromide ($MgBr_2$)-$MgSO_4$@CMS. Finally, the potential of the binary salt composite-based fluidized bed systems for space heating in buildings was evaluated and compared to traditional zeolite 13X-based systems.

2. Materials and methods

2.1. Selection of salts and porous matrix

In this work, $MgCl_2$ and $MgSO_4$ were selected as the impregnated salts, primarily because they both have high theoretical energy densities (e.g., 3.1 GJ/m^3 for dehydrating $MgCl_2{\cdot}6H_2O$ to $MgCl_2$ and 2.3 GJ/m^3 for $MgSO_4{\cdot}7H_2O$ to $MgSO_4{\cdot}H_2O$) [11], low costs (0.09 and 0.07 Euro/MJ) [55], and high deployment levels (7 and 9) [56]. Additionally, mixing salt hydrates with a common cation (Mg^{2+}) can help avoid undesirable reactions [32,35]. Anhydrous salts $MgCl_2$ and $MgSO_4$ were purchased from Fisher Scientific UK Ltd.

For fluidized-bed applications, composite materials should have good fluidizability to achieve an optimal fluidization state, which is essential for efficient heat charging and discharging processes. Moreover, a large pore volume and mesopore size are crucial to prepare salt composites with high salt loading levels and excellent hydration and dehydration performance. To meet these requirements, commercial mesoporous silica (CMS) from PQ Silicas UK Ltd, with particle sizes ranging from 150 to 300 μm, was selected due to its excellent fluidization characteristics without gas channeling or slugging issues. In contrast, many high-performance mesoporous materials, such as metal-organic framework (MOF), are available in fine powder form with particle sizes below 50 μm. They are difficult to fluidize due to strong inter-particle cohesion forces. Moreover, the CMS has an average pore size of 27.4 nm, a total pore volume of 1.79 cm^3/g, and a specific surface area of 283 m^2/g [57]. The large pore size and volume allow for the impregnation of salts up to 50 wt% while maintaining fast dehydration and hydration kinetics [57]. In comparison, traditional porous matrices such as silica gel and zeoltie 13X have much smaller particle sizes (below 10 nm) and lower salt loading capacities of up to 30 wt% [18]. Based on these considerations, CMS was chosen as the porous matrix for preparing the salt composite materials discussed in this paper.

2.2. Preparation of composite materials

The salt@CMS composites were prepared using the incipient wetness impregnation method [57]. In a typical procedure, 1 g of salt or a $MgCl_2$-$MgSO_4$ salt mixture was first dissolved in 20 mL of deionized water with stirring. Then, 1 g of CMS powder was added to the solution, which was kept at ambient temperature with continuous stirring until the water naturally evaporated. The resulting composite materials were then transferred to a vacuum oven and dried at 150 °C for 6 h. After cooling, the white powder was collected and stored for further use. Five different composite materials with a weight percentage of $MgCl_2$ in the salt mixture of 0% (pure $MgSO_4$), 25% ($MgCl_2/MgSO_4$ = 1:3), 50% ($MgCl_2/MgSO_4$ = 1:1), 75% ($MgCl_2/MgSO_4$ = 3:1) and 100% (pure $MgCl_2$) were prepared for further tests. The water adsorption performance of the salt composite materials was first evaluated by using thermogravimetric analysis (TGA-Q500, USA) with the weighting accuracy of ±0.1%, sensitivity <0.1 μg, and isothermal temperature accuracy of ±0.1 °C at 30 °C and 25 mbar H_2O. In a typical TGA analysis, 20–40 mg of sample was first dried at 150 °C in a flow of nitrogen (100 ml/min) for 45 min. Then the TGA sample chamber was cooled down to 30 °C and supplied with moisture at 25 mbar water vapour pressure. When the adsorption equilibrium was achieved, the sample was heated up again to 150 °C at a heating rate of 1 °C/min with the gas being switched back to dry nitrogen.

Based on the adsorption results obtained by TGA, the single-salt composites and the best-performing binary-salt composite were selected and prepared in a larger batch (30 g) for energy storage performance evaluation in a fluidized bed. The scaled-up preparation followed a similar incipient wetness impregnation method as previously described.

2.3. Experiment setup

The composite materials were further evaluated using the experimental setup shown in Fig. 1. The reactor was 3D-printed from Acrylonitrile butadiene styrene (ABS) filament, with a cylinder height of 300 mm and an inner diameter of 40 mm. Anhydrous particles were placed in the reactor and fluidized by compressed air entering from the cylinder bottom. To prevent particles escape, borosilicate glass filter discs (porosity grade 2) were mounted at both ends of the cylinder. Two PT100 probes were attached to the reactor using PTFE adaptors: one immersed in the particle bed at a height of 30 mm to measure the bed temperature, and the other positioned at a height of 110 mm to measure the outlet air temperature. To minimize heat loss, the reactor was covered with 26 mm thick nitrile rubber with a thermal conductivity of 0.034 W/m·K. Hygro-thermometers and pressure transmitters were installed upstream and downstream of the reactor to measure air humidity, temperature, and gauge pressure. All the sensors were connected to a data logger, with data recorded at 10-s intervals. The specific experimental procedures are as follows:

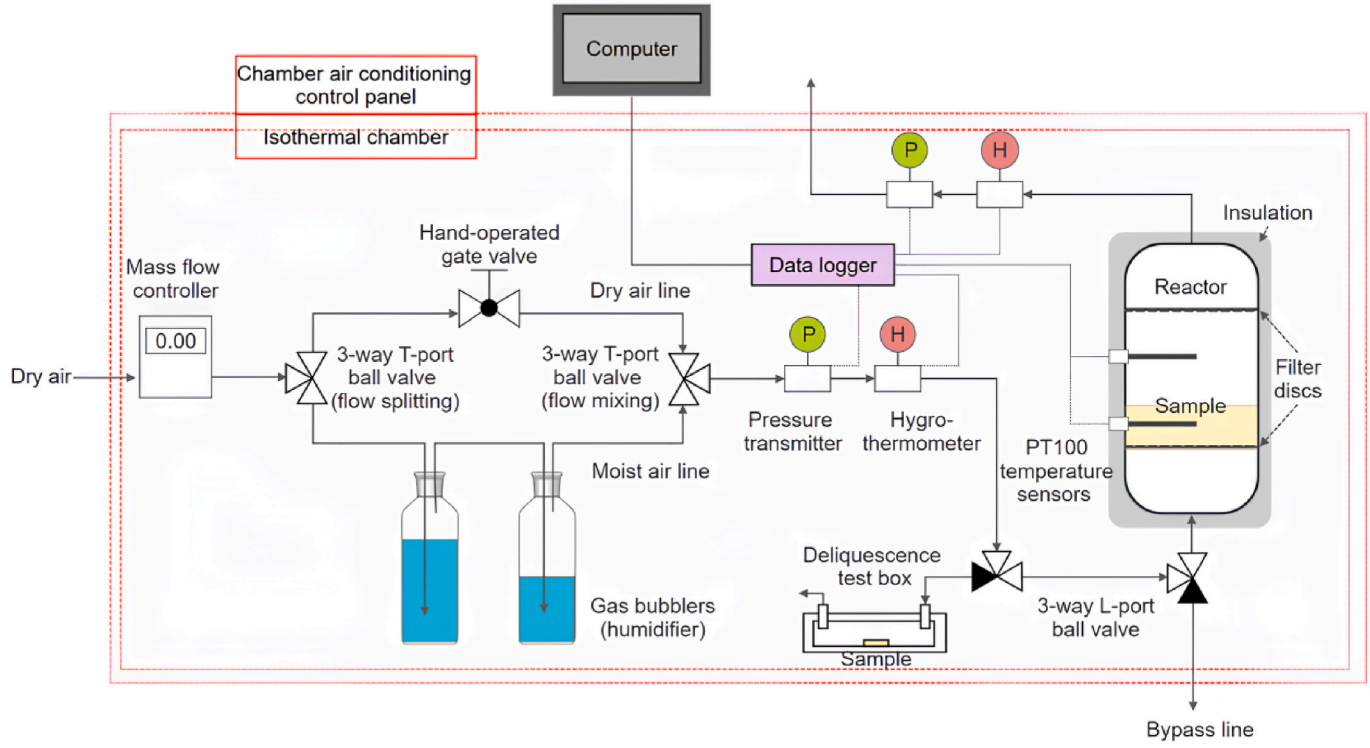

Fig. 1. Experimental setup for reactor-scale thermal analysis and fluidization tests.

(1) Prior to the fluidized-bed tests, the sample was dehydrated at 150 °C for 6 h, then cooled to ambient temperature under vacuum before being immediately transferred to the reactor for experimentation.
(2) A 30 g anhydrous sample was placed in the reactor and hydrated under controlled conditions. The flow rate was set to 6 L/min using a mass flow controller. The inlet air temperature was maintained at 30 ± 1.5 °C through a self-built isothermal chamber. The relative humidity was controlled at 60 ± 2.5% by mixing dry air with moist air (humidified through gas bubbling) and adjusting the gate valve in the dry air line.
(3) The experiment was terminated when the difference between the outlet and inlet air temperatures dropped to below 2 °C or when the experiment period exceeded 10 h.
(4) For parametric analysis, a series of hydration tests were carried out with varying flow rates from 2 to 8 L/min, temperatures from 20 to 35 °C, and RHs from 40 to 80%. N.B., for tests at RH ≥ 60%, moist air was initially directed to a deliquescence test box containing a small sample (0.15 g) to confirm no liquid leakage. Then, moist air was directed to the reactor by adjusting the 3-way L-port ball valves to the positions shown in Fig. 1 (White: open; Black: closed).
(5) The energy storage density (*ESD*) of the test material was calculated using **Equations (1-2)**.

More information about the experimental setup and parameter calculation methods are available in our previous publication [58]. The specifications of the sensors and system components are provided in Table 1.

$$Q_{dis} = \sum_{0}^{j=N} C_p\, q_m\, (T_{out}(t_i) - T_{in}(t_i))\Delta t \quad (1)$$

$$ESD = \frac{Q_{dis}}{m} \quad (2)$$

Table 1
Specification of the measurement equipment and accessories.

	Supplier and model number	Range	Accuracy
Hygro-thermometer	Rotronic HC2A-IE02	−100–200 °C 0–100% RH	±0.1 °C ±0.8% RH
Mass flow controller	Aalborg GFC37	0–30 L/min	±1% of full scale
PT100 sensor	Alphatemp Class A	−75–250 °C	±0.15 °C
Pressure transmitter	Jumo dTRANS p30	0–0.25 bar	±0.5% of full scale
Data logger	Omni Instruments DT85 Series 4		
3D printer	Original Prusa i3 MK3S		
3D printer filament	Verbatim transparent ABS	99 °C (heat deflection)	
PTFE adaptor	GPE scientific CG-1048-P-02		
Glass filter discs	Robu VitraPOR™ Ground Cylindrical, 50 mm	Porosity 2 (pore size 40–100 μm)	
Gas bubbler	DWK Life Sciences DURAN™		

Where Q_{dis} is the useful sorption heat during discharge process (kJ), C_p is the specific heat capacity of the airflow (kJ/kg·K); q_m is the mass flow rate of the airflow (kg/s); $T_{out}(t_i)$ is the outlet air temperature (K) measured at the time of t_i; $T_{in}(t_i)$ is the inlet air temperature (K) at the time of t_i; Δt is the time interval between two consecutive temperature measurements (s); N is the number of time intervals; m is the sample's weight (kg).

3. Results and discussion

3.1. Material characteristics

Water sorption capacity and desorption temperature are important

characteristics of thermochemical materials, which can be evaluated using TGA. Fig. 2(a) illustrates the performance of five salt composites tested under 30 °C and a partial moisture partial pressure of 25 mbar. It was found that the $MgSO_4$@CMS composite had the lowest water sorption capacity at 0.47 g/g of dry adsorbent, among all the composite materials, while the $MgCl_2$@CMS composite exhibited both a higher water sorption capacity, 1.07 g/g, and a faster water adsorption rate (also see Table 2). When mixing $MgCl_2$ and $MgSO_4$, the water uptake increased to 0.68 g/g as the ratio of $MgCl_2$ to $MgSO_4$ increased from 1:3 to 1:1, which was 45% higher than that of the $MgSO_4$@CMS composite. With a further increase of the $MgCl_2/MgSO_4$ ratio to 3:1, the water uptake significantly increased to 0.95 g/g, which was only about 10% lower than that of the $MgCl_2$@CMS composite, indicating that over-hydration might occur at a high $MgCl_2$ mass ratio under the experimental condition. In addition to water adsorption capacity, the water adsorption rate of the binary-salt composite also varied with the salt mixing ratio, falling between those of the single-salt composites. Among all the tested binary-salt composites, the $MgCl_2$-$MgSO_4$(1:1)@CMS composite exhibited the highest water adsorption rate.

In terms of desorption performance, the fraction of water absorbed in the material, denoted as C/C_0, is plotted as a function of desorption temperature in Fig. 2(b). Clearly, the addition of $MgCl_2$ to $MgSO_4$ significantly improved the dehydration kinetics of $MgSO_4$, all binary salt composites and $MgCl_2$ composites showed similar dehydration profile as the value of C/C_0 decreased to nearly 0% at temperatures below 150 °C, indicating the completion of dehydration. At lower temperatures, such as 80 °C, less than 30% of the water remained in the binary-salt composites, demonstrating that these composites can be effectively dehydrated using low-temperature heat sources.

Overall, the results demonstrate that the binary-salt composites inherit the unique features of both deliquescent and non-deliquescent salts, achieving effective water sorption and desorption. For fluidized-bed tests, the binary-salt composite with a 1:1 salt mixing ratio was selected due to its balanced performance in water sorption capacity, reaction kinetics, and stability at high RH levels.

3.2. Fluidization behaviour

The behaviour of fluidized beds can be understood through the Geldart's classification, which categorizes particles into Groups A, B, C, and D based on their size and density [59,60]. As demonstrated in our previous study [58], the CMS powder with diameters of 150–300 μm easily fluidized at low gas velocities and exhibited the characteristics of Geldart group A particles, such as smooth bed expansion before the occurrence of bubbling. The minimum flow rate required for fluidizing the CMS powder in a 40-mm-diameter reactor is approximately 0.5 L/min, equivalent to a minimum fluidization velocity (u_{mf}) of 6.6×10^{-3} m/s. In Fig. 3(a), the transition point where the CMS powder curve changes from inclined to level marks the minimum fluidization condition. Increasing the sample mass from 15 g to 30 g has a minor effect on u_{mf}, but nearly doubles the pressure drop across the particle bed.

Table 2
Total water uptake of the salt composites with a salt content of 50 wt%.

	$MgSO_4$@CMS	$MgCl_2$-$MgSO_4$@CMS			$MgCl_2$@CMS
		3:1	1:1	1:3	
Total water uptake (g/g)	1.07	0.95	0.68	0.57	0.47

For CMS powders impregnated with salt hydrates, they have similar particle sizes but higher particle densities, resulting in behaviour distinct from that of the pure CMS powder and aligning with the characteristics of Geldart group B particles [58]. Specially, the salt@CMS composite powder does not undergo significant bed expansion, and bubbles form at the onset of fluidization. Compared with the CMS powder, the salt@CMS composites require higher values of u_{mf}. Take $MgSO_4$-$MgCl_2$@CMS composite as an example. The required minimum flow rate is approximately 1 L/min and the u_{mf} is about 1.3×10^{-2} m/s, as indicated in Fig. 3(a).

For further clarity, the dimensionless pressure drop ($\Delta P/\Delta P_0$) was calculated and plotted against flow rate. Here, ΔP denotes the measured pressure drop across the bed, and ΔP_0 represents the pressure drop equal to the static weight of particles per unit area of the bed (234 Pa for a 30 g sample) [61]. When $\Delta P/\Delta P_0 = 1$ the entire bed is considered to be fully fluidized. As can be seen from Fig. 3(b), before reaching 1 L/min, the values of $\Delta P/\Delta P_0$ are below 1, indicating the bed remains static. When the flow rate exceeds 1 L/min, the bed transitions to a fluidized state.

At higher flow rates, such as 2 L/min, and the pressure drop remains almost constant, while bubbling and solid mixing become more vigorous. Fig. 4 shows the growth, coalescence and collapse of bubbles, tracked using a slow-motion camera. The motion of gas bubbles induced particle movement and circulation. This promotes heat transfer between solids and between solid and gas, leading to a uniform temperature distribution both radially and axially in the particle bed. This is confirmed by a follow-up hydration experiment, with thermal images captured using a FLIR E6 infrared camera. As shown in Fig. 5, the solid bed heated up when reacting with moist air, and the temperature distribution remained uniform across the bed section during hydration.

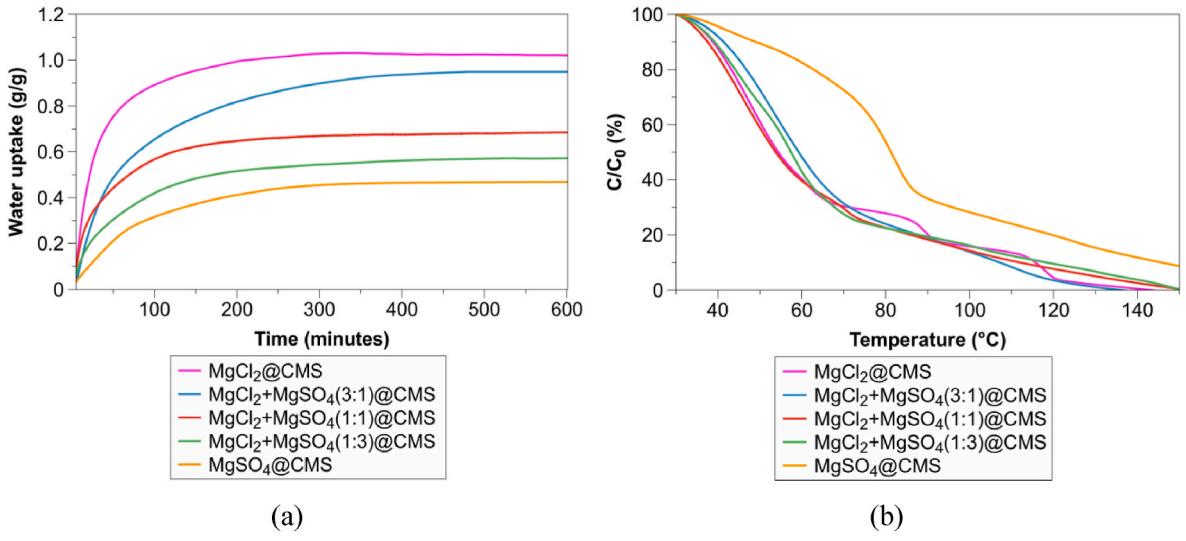

Fig. 2. TGA results including (a) sorption performance and (b) desorption performance of the salt composites with a salt content of 50 wt%.

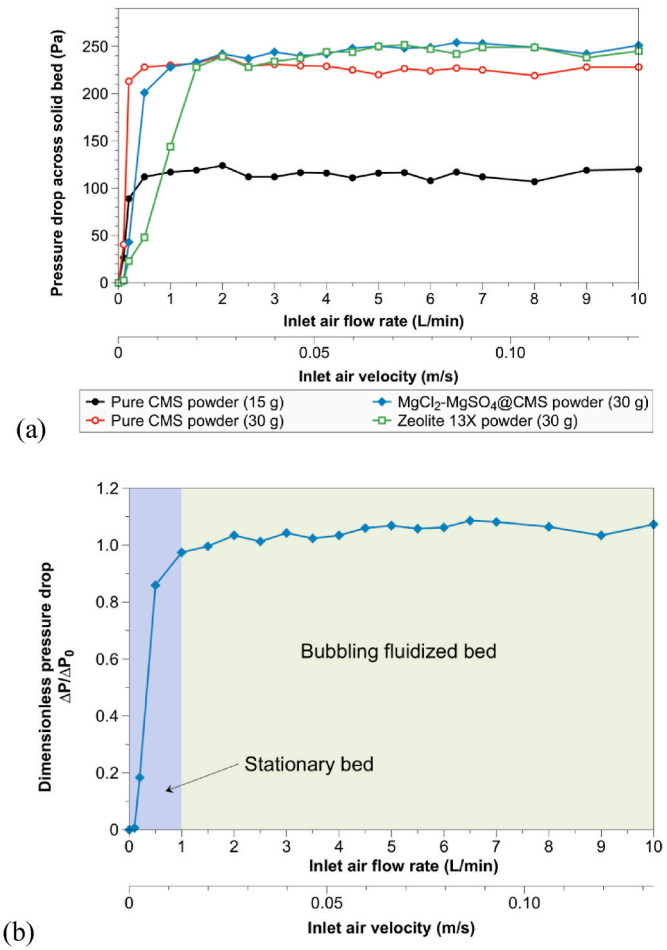

Fig. 3. (a) Pressure drops across the beds of different sorption materials; (b) dimensionless pressure drop of the $MgSO_4$-$MgCl_2$@CMS composite.

Additional tests were conducted using another Geldart Group B powder, zeolite 13X, with particle sizes ranging from 212 to 425 μm and a minimum fluidization velocity of 2.6×10^{-2} m/s. Similar bubbling fluidization behaviors were observed (see Fig. S1).

3.3. Thermal characteristics at the reactor scale

Generally, the water sorption capacity and energy density of thermochemical materials increase with higher humidity. However, this does not necessarily imply that higher humidity is optimal for heat storage applications, due to potential leakage and agglomeration problems of salt hydrates [33]. Therefore, it is crucial to select an appropriate humidity level to balance energy density and material stability. To address this, an initial leakage assessment was conducted with a small sample mass exposed to different RH levels, ranging from 40% to 80%, at 30 °C.

As illustrated in Fig. 6, the single-salt $MgCl_2$@CMS composite maintained its powdery form at an RH of 60%. However, upon exposure to an RH of 80%, the white particles became wet and translucent within an hour, and completely liquefied within 3 h. In contrast, the single-salt $MgSO_4$@CMS composite retained its dryness and structural integrity at 80% RH, consistent with expectations, given that the deliquescence relative humidity (DRH) of magnesium sulphate heptahydrate ($MgSO_4 \cdot 7H_2O$) is high at 90% at 30 °C [25,32]. Despite some wetness, the binary-salt $MgCl_2$-$MgSO_4$@CMS composite did not turn into liquid after 10 h of hydration. This may be due to $MgSO_4$ forming a protective layer around the $MgCl_2$ particles, which hinders direct contact with moisture and consequently decreases the water sorption rate [38]. The salt-mixing effect on hydration rate is confirmed by the TGA test (see Fig. 2). Posern and Kaps [32] found that reducing the proportion of $MgCl_2$ in $MgCl_2$-$MgSO_4$ mixture from 100% to 40% resulted in an increase in DRH from 33% to around 60%. Accordingly, it can be deduced that the $MgCl_2$-$MgSO_4$@CMS composite, which has a higher DRH and a lower water sorption rate compared to the $MgCl_2$@CMS composite, forms less salt solution within the pores of CMS. This reduces the risk of exceeding the pore volume and causing liquid leakage.

Based on these findings, the maximum RH for subsequent reactor-scale tests with the $MgCl_2$@CMS composite was limited to 60%, whereas for the $MgSO_4$@CMS composite and the binary-salt composite, it was set at 80%.

Following the preliminary test, a larger quantity of the composite samples (30 g) was tested at the reactor scale. Fig. 7(a) shows that at 60% RH and 30 °C, the single-salt $MgCl_2$@CMS composite experienced a rapid increase in bed temperature, peaking at 60.1 °C within 1 h. The temperature then declined at different rates: rapidly from 1:00 to 3:00 and more slowly from 3:00 to 10:00. This behavior is attributed to the $MgCl_2$ chemisorption - deliquescence - dissolution - dilution process [21], which affects water sorption and heat release. Specifically, the initial temperature rise is attributed to the high hydration rate of $MgCl_2$, associated with particle surface adsorption (chemisorption). Subsequently, salt deliquescence and dissolution may partially block the micropores, reduce the solid-gas contacting area, and limit moisture access to the salt inside pores. The reduced rate of water adsorption was insufficient to sustain high heat output, resulting in a sharp temperature drop. As water intake continued, the saturated salt solution inside pores became diluted, resulting in weaker liquid absorption and gradually reduced heat output. Consequently, the bed temperature slowly decreased to the inlet air temperature (~30 °C).

At 60% RH, the binary-salt $MgCl_2$-$MgSO_4$@CMS composite reached a lower maximum bed temperature of 50.4 °C and experienced a temperature decline 30 min earlier than the $MgCl_2$@CMS composite. This is likely because the binary-salt composite contains less $MgCl_2$, resulting in a lower heat release rate. When the RH was reduced to 40%, the temperature variation trends remains unchanged, with the maximum bed temperatures dropping to 45.2 °C for the binary-salt composite and 51.0 °C for the single-salt composite. Increasing the RH to 80% achieved

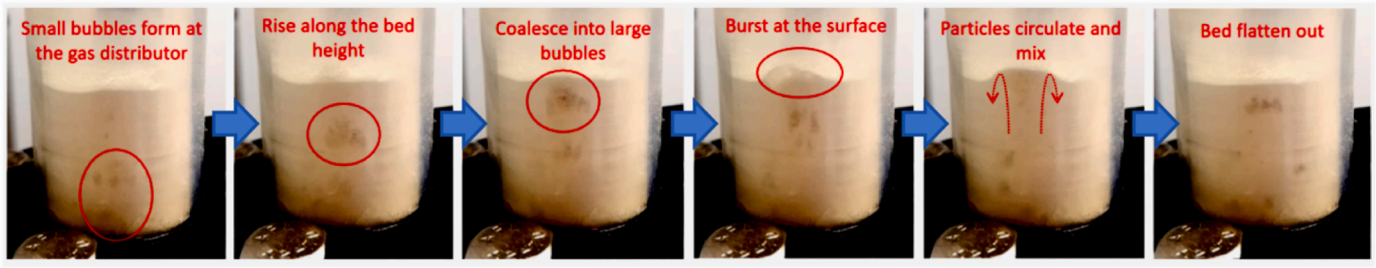

Fig. 4. Photos showing the fluidization behaviour of the $MgSO_4$-$MgCl_2$@CMS composite at a flow rate of 2 L/min. Small bubbles formed at the reactor bottom, coalesced into large bubbles as they rose, and finally collapsed at the top surface of the fluidized bed (left to right).

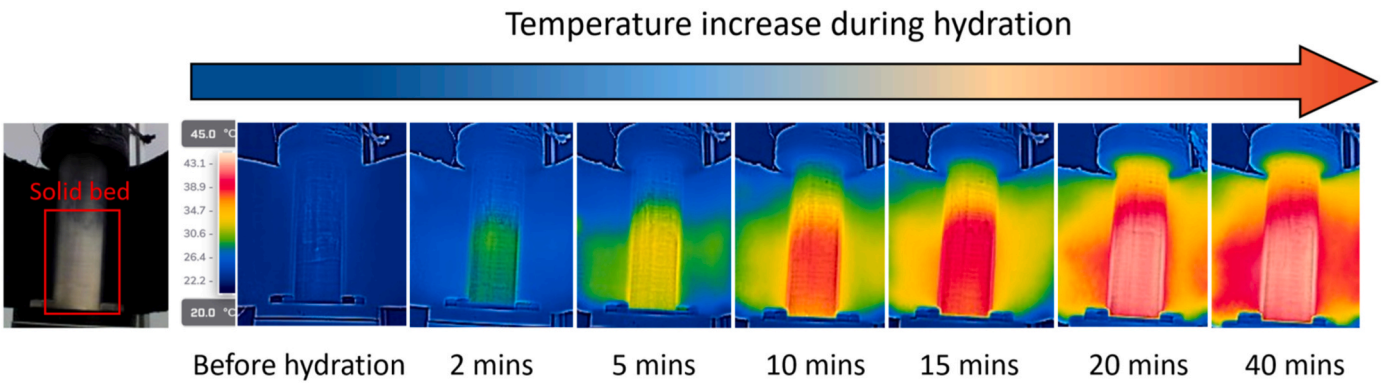

Fig. 5. Thermal images illustrating the uniform temperature distribution of the solid bed when it was fluidized and hydrated with moist air at a flow rate of 6 L/min, RH of 60%, and 23 °C.

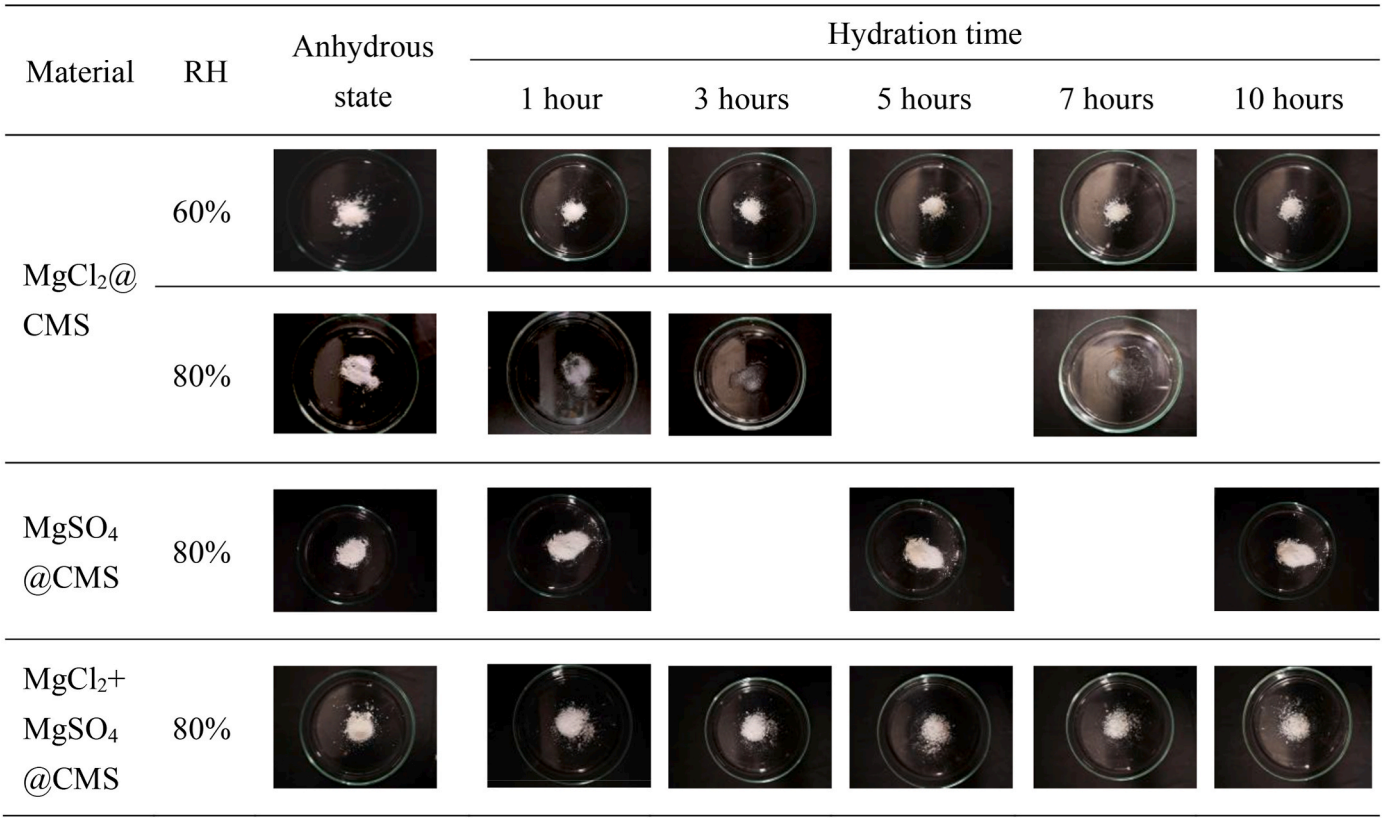

Fig. 6. Photos of the salt composites in a small sample mass (0.15 g) before and after hydration in the deliquescence test box.

a maximum bed temperature of 54.5 °C for the $MgCl_2$-$MgSO_4$@CMS composite (see Fig. 7(b)), and the duration during which the temperature lifts exceeded 5 °C was extended from 3 to 5 h. Although using higher RHs is expected to further increase the discharge temperature and useful heating period, the stabilization effect may be compromised as $MgSO_4$ begins to deliquesce at 90% RH at 30 °C.

At 60% RH, the single-salt $MgSO_4$@CMS composite reached a maximum bed temperature of 41.7 °C and offered a useful heating period of only 40 min. For the next 9 h, the temperature lift remained steady at around 2 °C. This aligns with the reported slow kinetics and poor rehydration ability of $MgSO_4$ [62]. Initially, $MgSO_4$ quickly adsorbs water vapour; however, as a layer of hydrated salt ($MgSO_4{\cdot}xH_2O$) forms on the surface, it hinders further water vapour diffusion, reducing the adsorption rate. Increasing the RH to 80% ameliorated the situation, with the maximum bed temperature rising to 46.5 °C and the useful heating period extended to 5 h. The improvements are likely due to enhanced kinetics at higher water vapour pressure, which increases the driving force for water diffusion through the hydrated layer. Additionally, at 80% RH and 30 °C, $MgSO_4{\cdot}7H_2O$ (epsomite) forms, which enhances the water sorption compared to $MgSO_4{\cdot}6H_2O$ (hexahydrite) formed at 60% RH [25,63].

Table 3 presents the total water uptake (W_t), energy storage density (*ESD*), and maximum temperature lift for the three salt composite materials at specific RH levels. At 60% RH, the binary-salt composite showed a total water uptake of 0.46 g/g, which is between the single-salt composites, $MgCl_2$@CMS (0.78 g/g) and $MgSO_4$@CMS (0.24 g/g). These values are lower than those from TGA tests (Table 2), probably due to factors such as incomplete reactions, slower kinetics, and particle agglomeration in macro-scale systems [13,64].

For hydration at 40% RH, the binary-salt composite achieved an *ESD*

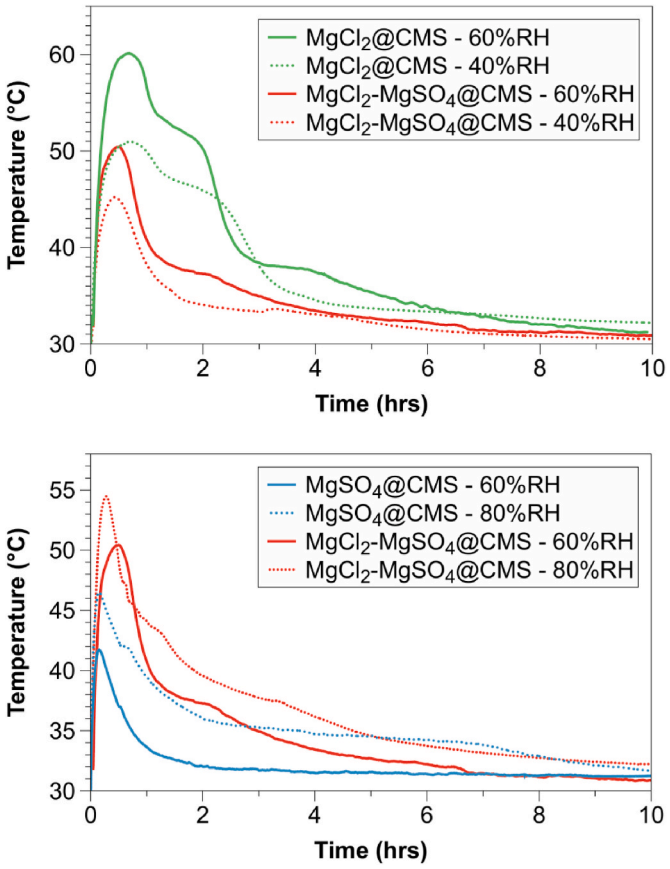

Fig. 7. Comparison of bed temperatures of the $MgCl_2$-$MgSO_4$@CMS composite with (a) the $MgCl_2$@CMS composite hydrated at 40% RH and 60% RH, and with (b) the $MgSO_4$@CMS composite hydrated at 60% RH and 80% RH.

of 388 kJ/kg. This increased to 687 kJ/kg at 60% RH, amounting to 52% of the *ESD* of the $MgCl_2$@CMS composite (1319 kJ/kg). At 80% RH, the ESD of the binary-salt composite further rose to 1018 kJ/kg, surpassing the $MgSO_4$@CMS composite (767 kJ/kg) by 32%. It is important to note that these *ESD* values were calculated based on the air temperature lifts, which are lower than the bed temperature lifts, likely due to heat absorption and loss along the reactor height. The *ESD* values could be even higher with improved reactor sizing and insulation. The binary-salt composite maintained consistent thermal characteristics over 10 cycles at 60% RH and 30 °C during hydration, and 150 °C during dehydration. When the RH was increased to 80%, the stability of material decreased slightly, resulting in less than a 10% reduction in *ESD* after 10 cycles (see Fig. 8).

Overall, the binary-salt composite showed satisfactory temperature lifts and ESDs under high humidity conditions. Although the values are lower than those of the $MgCl_2$@CMS composite, the binary-salt composite demonstrated good stability and less agglomeration during hydration (see Fig. 9). This reduced agglomeration is particularly beneficial for fluidized-bed applications, where consistent material flow and minimal particle clustering are crucial for optimal performance.

3.4. Parametric analysis regarding different operating conditions

Section 3.3 highlights that the heat storage performance of the composite materials improves at higher RH, indicating that the moisture content of inlet air significantly influence the water sorption and heat output. The section further explores the behaviour of the $MgCl_2$-$MgSO_4$@CMS composite in the fluidized-bed TCES system when operating at varying flow rates and hydration temperatures.

As discussed in Section 3.2, the solid bed transitioned to a bubbling fluidization regime at flow rates exceeding 1 L/min. For thermal analysis, flow rates of 2, 4, 6, and 8 L/min were selected to ensure effective solid-gas mixing and reaction. Higher flow rates beyond 8 L/min were avoided due to strong entrainment effects and turbulence, which could cause large pressure fluctuations and operational instability. Fig. 10(a) shows that increasing the flow rate from 2 to 4 L/min raised the maximum temperature lift from 15.7 to 23.5 °C, with a steeper curve gradient, indicating faster hydration due to the increased moisture entering the reactor. However, at 6 L/min, the maximum temperature lift decreased to 21.8 °C, and further declined to 18.4 °C at 8 L/min. This reduction may be due to rapid heat removal at high flow rates, which prevented heat accumulation in the solid bed. Additionally, the larger volume of air being heated and the greater convective heat loss at higher flow rates further contributed to the diminished temperature lifts. A similar phenomenon was observed by Bardy et al. [52] in a zeolite-13X fluidized bed, where increasing the flow rate from 10 to 30 L/min reduced both the temperature lift and the heating time. The *ESD* of the binary salt composite was raised from 203 to 712 kJ/kg as the flow rate increased from 2 to 8 L/min (see Fig. 10(b)). This improvement is expected, as higher flow rates allow the reaction to approach completion, fully extracting the stored energy. To balance temperature lift and *ESD*, 6 L/min was identified as the optimal flow rate and used in subsequent investigations on the effect of hydration temperature (T_h).

Hydration tests were conducted at temperatures of 21, 30, and 35 °C,

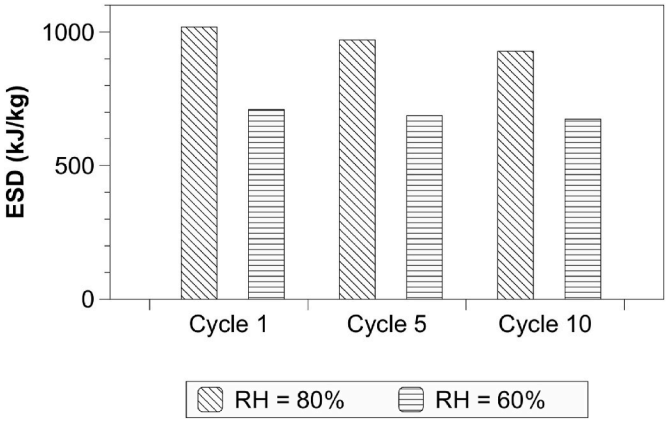

Fig. 8. Performance of the $MgCl_2$-$MgSO_4$@CMS composite over multiple cycles of hydration (60% or 80% RH, 30 °C, and 6 L/min) and dehydration (150 °C).

Table 3
Energy storage density *(ESD)*, total water uptake (W_t), and maximum temperature lifts for the fluidized bed (ΔT_{bed}) and airflow (ΔT_{air}), derived for the salt composites at different RH levels.

Performance indicator	RH = 40%				RH = 60%				RH = 80%			
	ESD (kJ/kg)	W_t (g/g)	ΔT_{bed}, (°C)	ΔT_{air} (°C)	*ESD* (kJ/kg)	W_t (g/g)	ΔT_{bed} (°C)	ΔT_{air} (°C)	*ESD* (kJ/kg)	W_t (g/g)	ΔT_{bed} (°C)	ΔT_{air} (°C)
$MgCl_2$@CMS	830	0.50	21.3	15.9	1319	0.78	31.5	24.6				
$MgCl_2$-$MgSO_4$@CMS	388	0.24	15.5	11.4	687	0.46	21.8	16.5	1018	0.64	24.7	18.8
$MgSO_4$@CMS					368	0.24	12.6	10.0	767	0.47	17.4	14.7

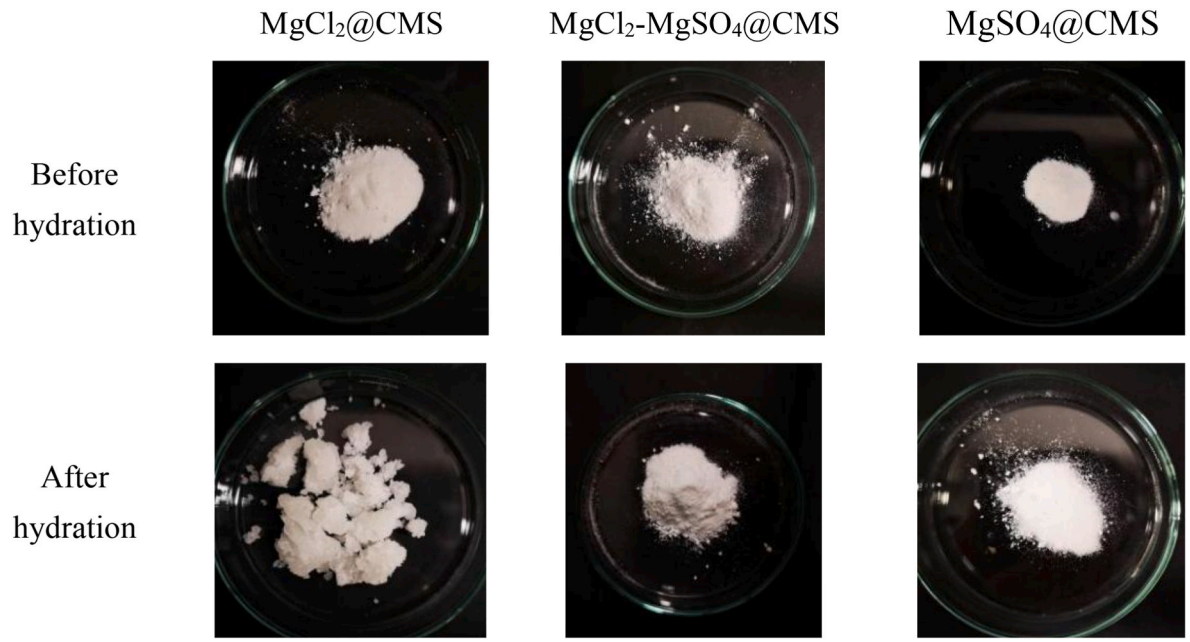

Fig. 9. Photos showing the appearances of the salt composite materials before hydration and after 10-h hydration at 60% RH, 30 °C, and 6 L/min.

with the RH maintained at 60%. These conditions correspond to partial water vapour pressures (P_w) of 15, 25, and 34 mbar, respectively. As shown in Fig. 10(c), hydration at 21 °C resulted in a maximum temperature lift of 15.3 °C, while at 35 °C, it reached 23.6 °C. This difference can be attributed to the higher P_w at elevated temperatures, which provides a greater driving force for moisture diffusion into the particles, leading to a higher rate of heat discharge. In terms of *ESD*, the value increased from 593 to 687 kJ/kg as the hydration temperature rose from 21 to 30 °C, but then decreased to 570 kJ/kg at 35 °C (see Fig. 10(d)). The lower *ESD* at 35 °C may be attributed to the reduced water sorption, which was 0.38 g/g compared to 0.46 g/g at 30 °C.

According to water vapour sorption isotherms reported in the literature [65,66], the water uptake of salt composites decreases at lower T_h and increases at higher P_w. To validate this, additional hydration tests were conducted at a constant P_w (~25 mbar) with hydration temperatures of 21, 30 and 35 °C. As confirmed in Fig. 10(e–f), both the temperature lift and *ESD* decreased with increasing T_h. A comparison between Fig. 10(c–d) and Fig. 10(e–f) reveals that, at the same hydration temperatures, samples tested at higher levels of P_w exhibited higher temperature lifts and *ESD*s. Notably, when hydrated at 21 °C and 24 mbar, the *ESD* reached 1204 kJ/kg, more than twice that observed at 21 °C and 15 mbar. This may be attributed to the deliquescence and dissolution of $MgSO_4{\cdot}7H_2O$ taking place at the high RH level (97%), which substantially enhanced the water sorption capacity of the mixed salt hydrates.

In summary, the thermal performance of the binary salt composite can be improved by optimizing the flow rate and employing a high partial water vapour pressure. However, the latter is constrained by the selected hydration temperature. Achieving high P_w at low hydration temperatures necessitates high RH levels, which may lead to material stability issues and condensation in the system. Conversely, high P_w at elevated hydration temperatures is feasible but may result in lower water uptake and reduced *ESD*. In this test, hydration conditions of a 6 L/min flow rate, 30 °C temperature, and 60% RH produced satisfactory results and were thus used for further material comparison in the subsequent section. For practical applications, it is essential to explore various combinations of system operating conditions to determine the optimal balance for maximizing material performance.

3.5. A comparison between binary-salt composites with previously reported materials

The above findings demonstrate the feasibility of using a binary-salt composite in powder form for fluidization and heat storage applications. The $MgCl_2$-$MgSO_4$@CMS composite shows great potential by merging the benefits of the $MgCl_2$@CMS composite—such as fast reaction kinetics, high water uptake, and substantial temperature lift—with the advantages of the $MgSO_4$@CMS composite, including reduced particle agglomeration. This suggests that combining $MgSO_4$ with other chloride-based deliquescent salts, such as LiCl and $SrCl_2$, could offer similar benefits and potentially improve overall performance compared to using each salt individually. Relevant studies on LiCl-$MgSO_4$ mixture [36] and $SrCl_2$-$MgSO_4$ mixture [38] can support this hypothesis. $MgBr_2$, although being highly deliquescent (DRH = 31% at 25 °C [67]), has not been extensively explored in mixed-salt composite development. This section introduces a new binary-salt composite, $MgBr_2$-$MgSO_4$@CMS, containing 50 wt% salts with a 1:1 mixing ratio. TGA test results revealed that the $MgBr_2$-$MgSO_4$@CMS composite absorbed moisture more rapidly than the $MgSO_4$@CMS composite, as evidenced by the steeper curve gradient, and achieved a higher water uptake compared to the $MgBr_2$@CMS composite, as presented in Fig. 11(a). Reactor-scale tests demonstrated that the binary-salt composite reached a maximum discharge temperature of 49 °C and an *ESD* of 570 kJ/kg, outperforming its single-salt counterparts, as shown in Fig. 11(b) and Table 4. The enhanced performance might be due to a synergistic effect between the two salts. For instance, $MgBr_2$ in the salt-mixture layer acted as a 'water pump', facilitating the diffusion of water molecules to the unhydrated $MgSO_4$, thereby overcoming kinetic hindrances and contributing to a higher temperature lift. The presence of $MgBr_2$ solution may also promote the formation of higher $MgSO_4$ hydrates, such as $MgSO_4{\cdot}7H_2O$, which could extract more heat stored in anhydrous $MgSO_4$, thereby improving the *ESD*. A similar synergistic effect may occur in the $MgCl_2$-$MgSO_4$@CMS composite; however, it showed intermediate performance in terms of temperature lift and *ESD* compared to the individual $MgCl_2$ and $MgSO_4$ composites. This is likely due to the significantly higher water sorption capacity of $MgCl_2$ compared to $MgBr_2$. Reducing the $MgCl_2$ salt content by half may have led to a substantial decrease in water sorption, which could outweigh the benefits of the synergistic interaction between $MgCl_2$ and $MgSO_4$, resulting

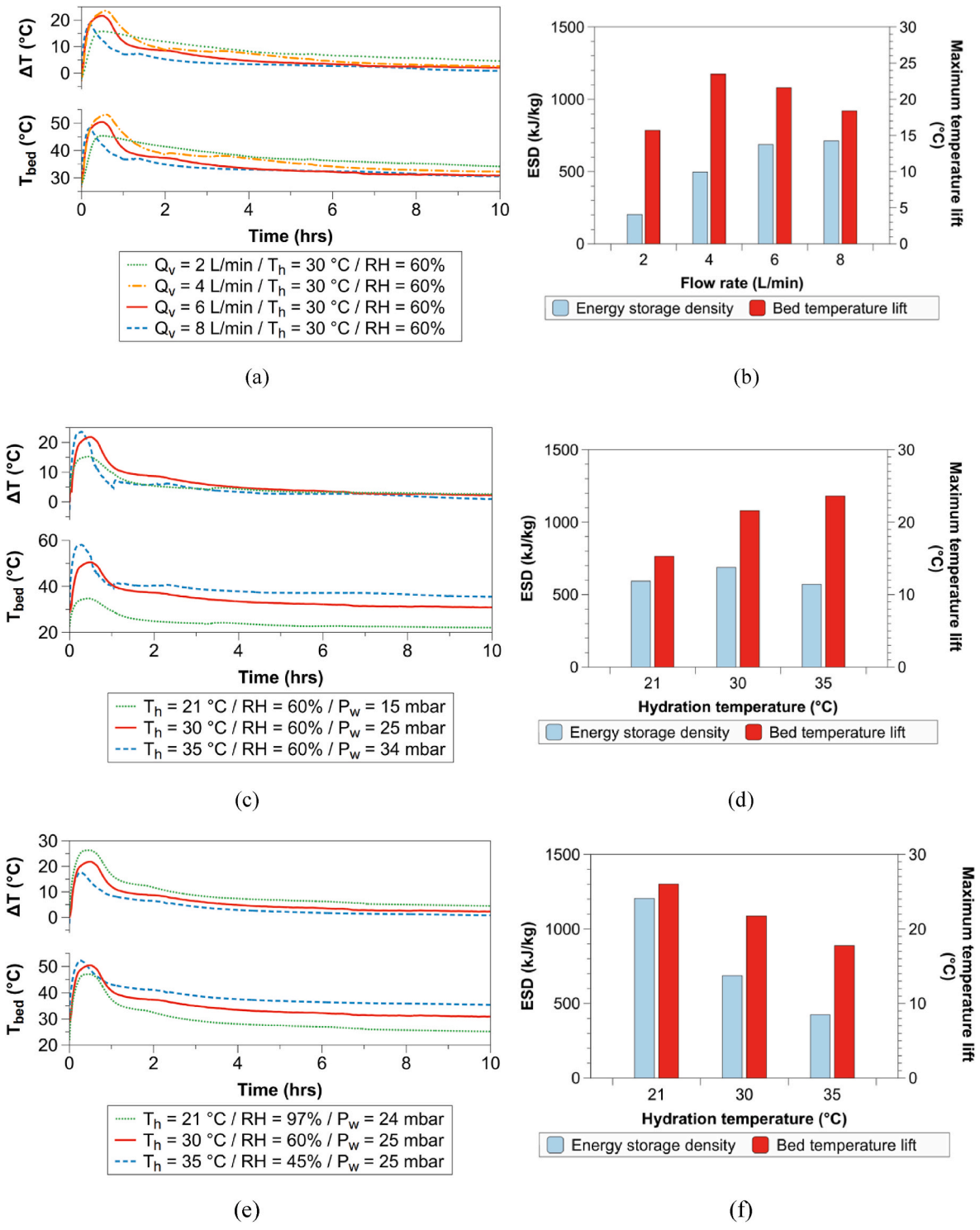

Fig. 10. Bed temperature (T_{bed}), temperature lift (ΔT), *ESD,* and maximum temperature lift of the $MgCl_2$-$MgSO_4$@CMS composite during hydration at (a–b) flow rates between 2 and 8 L/min, (c–d) temperatures ranging from 21 to 35 °C with similar RH levels, and (e–f) temperatures between 21 and 35 °C with comparable partial water vapour pressures (P_w).

in the observed intermediate performance of the binary-salt hydrate.

Table 4 compares the system-level performance of the single- and binary-salt composites investigated in this study with those reported in literature. The composite materials developed here are intended for use in fluidized beds for low-temperature heat storage and space heating in buildings. As shown, all proposed materials can be regenerated at a temperature of 150 °C and provide a maximum air temperature lift exceeding 10 °C, except for the $MgSO_4$@CMS and $MgBr_2$@CMS single-salt composites. The $MgCl_2$-$MgSO_4$@CMS binary-salt composite achieves an *ESD* of 1018 kJ/kg, with a maximum bed temperature of 54 °C and a maximum outlet air temperature of 48 °C, when hydrated at 80% RH and dehydrated at 150 °C. The *ESD* value surpasses that of zeolite 13X and many salt@zeolite composites in the literature, which typically require high charge temperatures (200–250 °C) to achieve *ESDs* close to 1000 kJ/kg. Under similar hydration and dehydration conditions, the $MgCl_2$-$MgSO_4$@CMS composite in a fluidized bed reactor offers lower

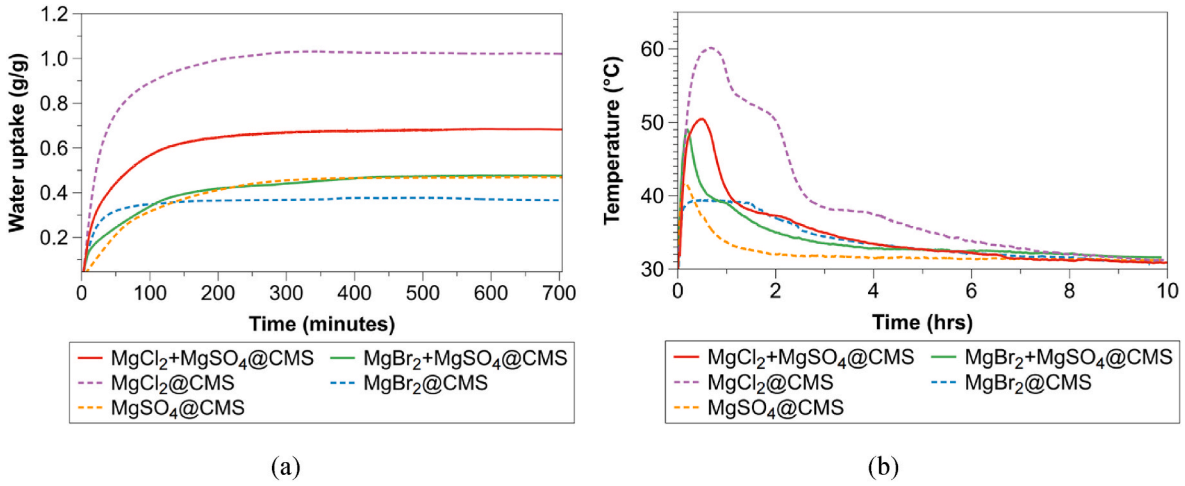

Fig. 11. Comparison of the single-salt and binary-salt composites in terms of (a) water sorption measured using TGA, and (b) discharge temperature measured at the reactor scale under the conditions of 6 L/min flow rate, 30 °C temperature, and 60% RH.

Table 4
Summary of the reactor-scale performance of TCES materials from this study and the literature.

Thermochemical material			Reactor prototype		System operating conditions				*ESD* (kJ/kg)	T_{max} (°C)	Refs
Salt	Porous matrix	Salt content (wt %)	Reactor type	Sample weight (kg)	T_h (°C)	RH (%)	Q_v (L/min)	T_d (°C)			
$MgCl_2$-$MgSO_4$	CMS	50 (1:1)	Fluidized	0.03	30	40	6	150	388	45[b]/41[a]	This study
					30	60	6	150	687	51[b]/45[a]	
					30	80	6	150	1018	54[b]/48[a]	
$MgBr_2$-$MgSO_4$	CMS	50 (1:1)	Fluidized	0.03	30	60	6	150	570	49[b]/43[a]	
$MgCl_2$	CMS	50	Fluidized	0.03	30	60	6	150	1319	60[b]/53[a]	
$MgSO_4$	CMS	50	Fluidized	0.03	30	60	6	150	368	42[b]/39[a]	
$MgBr_2$	CMS	50	Fluidized	0.03	30	60	6	150	473	39[b]/37[a]	
$CaCl_2$	CMS	50	Fluidized	0.03	30	60	6	150	1508	58[b]/50[a]	[58]
–	Zeolite 13X	–	Fluidized	0.025	25	70	25	200	776	48[a]	[52]
–	Zeolite 13X	–	Fixed	0.025	25	70	25	200	912	58[b]	[52]
$CaCl_2$	Vermiculite	67	Fixed	0.125	20	75	5	120	–	45[b]/30[a]	[48]
$MgSO_4$	Zeolite 13X	12.9	Fixed	0.2	20	56	10	150	433	41[a]	[23]
$MgSO_4$	Zeolite 13X	15	Fixed	8.5	25	–	–	250	551	92[b]	[25]
$MgCl_2$-$CaCl_2$	Zeolite 13X	15 (1:1.5)	Fixed	9	15–20	90	0.8 kg/s	130	719	61–66[a]	[42]
$SrCl_2$	Silica gel	10	Fixed	0.8	25	70	50	120	308	53[b]/41[a]	[54]
$MgSO_4$-$CaCl_2$	Vermiculite	55 (1:2)	Fixed	1.3	17–19	70–80	0.02 kg/s	200	1213	41–43[a]	[37]

[a] Maximum outlet air temperature.
[b] Maximum bed or sorbent temperature.

maximum temperature lifts but longer discharging period (>35 °C), compared to the same mass (30 g) of zeolite 13X powders in a fluidized-bed reactor (see Fig. S2) and zeolite 13X pellets in a packed-bed reactor (see Fig. S3). The energy density of zeolite 13X pellets reaches 201 kJ/kg at 80% RH, which is one fifth of that of the binary-salt composite. Accordingly, the binary salt composite-based fluidized bed system is well-suited for applications that do not require high temperature but involve long operation periods, such as space heating, and is a viable alternative to zeolite-based systems due to its greater heat storage capacity.

4. Conclusions

This study introduces a novel binary-salt composite, $MgCl_2$-$MgSO_4$@CMS, for use in fluidized-bed systems for low-temperature thermochemical energy storage. The composite consists of commercial mesoporous silica (CMS) with $MgCl_2$ and $MgSO_4$ in a mass ratio of 2:1:1. The material was evaluated at both the material level using Thermogravimetric analysis (TGA) and at the system level using a prototype fluidized-bed system. The binary-salt composite exhibits a water sorption capacity of 0.68 g/g at 60% relative humidity and 30 °C. The water uptake and reaction kinetics can be adjusted by varying the $MgCl_2$ and $MgSO_4$ mixing ratio. At the reactor scale, the binary-salt composite powder demonstrates excellent fluidization characteristics with a low minimum fluidization velocity (u_{mf}) of 1.3 × 10^{-2} m/s. Moreover, the bubbling fluidization ensures fast heat and mass transfer, efficient moisture sorption, and uniform temperature distributions during hydration. This promotes effective heat discharging performance. For instance, a temperature lift of up to 21.8 °C and an *ESD* of 687 kJ/kg were achieved when the binary-salt composite is hydrated at 30 °C, 60% RH, a partial water vapour pressure (*Pw*) of 25 mbar, and a flow rate of 6 L/min. Increasing the RH to 80% results in a higher *ESD* of 1018 kJ/kg. The parametric analysis shows that the temperature lift increases with higher hydration temperatures at a constant RH but decreases at higher hydration temperatures with a constant *Pw*. The binary-salt composite demonstrates good stability over 10 hydration-dehydration cycles and exhibits less agglomeration compared to the $MgCl_2$@CMS single salt composite. Overall, the $MgCl_2$-$MgSO_4$@CMS binary-salt composite exhibits excellent water sorption and heat storage performance.

Nevertheless, the material stability was found to slightly decrease

after more than 10 hydration cycles under high humidity conditions (80% RH). This is likely due to minor liquid leakage caused by the excessive formation of salt solution, exceeding the pore volume. Therefore, further modifications to the material's microstructure and composition are needed to enhance its stability, such as adjusting the salt mixing ratio and employing polymeric stabilization methods [68, 69]. For building applications, the fluidized bed reactor will also be optimized in terms of geometry and integration with key components, including heat exchangers, gas distributors, and solid feeding systems, to maximize efficiency and achieve a high coefficient of performance (COP). Future work will also involve designing a multi-stage cascade system that integrates reactors with different adsorbents, including binary salt hydrates, CSPMs, or zeolites, to leverage the unique properties of each sorbent and improve heat storage performance.

CRediT authorship contribution statement

Xiao Liu: Writing – review & editing, Writing – original draft, Methodology, Investigation, Formal analysis, Conceptualization. **Fangming Yang:** Writing – review & editing, Writing – original draft, Methodology, Investigation. **Xin Liu:** Writing – review & editing, Methodology, Investigation, Conceptualization. **Haomin Wang:** Investigation, Formal analysis. **Yupeng Wu:** Writing – review & editing, Supervision, Resources, Project administration, Methodology, Funding acquisition, Conceptualization.

Declaration of competing interest

The authors declare the following financial interests/personal relationships which may be considered as potential competing interests:

Yupeng Wu reports financial support was provided by Engineering and Physical Sciences Research Council. If there are other authors, they declare that they have no known competing financial interests or personal relationships that could have appeared to influence the work reported in this paper.

Acknowledgement

This work was supported by the Engineering and Physical Sciences Research Council, UK [grant number EP/S030786/1].

Appendix A. Supplementary data

Supplementary data to this article can be found online at https://doi.org/10.1016/j.renene.2024.121668.

References

[1] R. Köll, W. van Helden, G. Engel, W. Wagner, B. Dang, J. Jänchen, H. Kerskes, T. Badenhop, T. Herzog, An experimental investigation of a realistic-scale seasonal solar adsorption storage system for buildings, Sol. Energy 155 (2017) 388–397.
[2] S. Wang, P.-J. Hoes, J.L.M. Hensen, O.C.G. Adan, P.A.J. Donkers, A design optimization method for solar-driven thermochemical storage systems based on building performance simulation, J. Energy Storage 72 (2023) 108354.
[3] D. Stitou, N. Mazet, S. Mauran, Experimental investigation of a solid/gas thermochemical storage process for solar air-conditioning, Energy 41 (1) (2012) 261–270.
[4] W. Li, X. Ling, Performance analysis of a sorption heat storage-photocatalytic combined passive solar envelope for space heating and air purification, Energy 280 (2023) 128189.
[5] A. Palacios, C. Barreneche, M.E. Navarro, Y. Ding, Thermal energy storage technologies for concentrated solar power – a review from a materials perspective, Renew. Energy 156 (2020) 1244–1265.
[6] N. Yu, R.Z. Wang, L.W. Wang, Sorption thermal storage for solar energy, Prog. Energy Combust. Sci. 39 (5) (2013) 489–514.
[7] X. Zhang, M. Li, W. Shi, B. Wang, X. Li, Experimental investigation on charging and discharging performance of absorption thermal energy storage system, Energy Convers. Manag. 85 (2014) 425–434.
[8] R. van Alebeek, L. Scapino, M.A.J.M. Beving, M. Gaeini, C.C.M. Rindt, H. A. Zondag, Investigation of a household-scale open sorption energy storage system based on the zeolite 13X/water reacting pair, Appl. Therm. Eng. 139 (2018) 325–333.
[9] K. Johannes, F. Kuznik, J.-L. Hubert, F. Durier, C. Obrecht, Design and characterisation of a high powered energy dense zeolite thermal energy storage system for buildings, Appl. Energy 159 (2015) 80–86.
[10] M. Gaeini, R.v. Alebeek, L. Scapino, H.A. Zondag, C.C.M. Rindt, Hot tap water production by a 4 kW sorption segmented reactor in household scale for seasonal heat storage, J. Energy Storage 17 (2018) 118–128.
[11] P.A.J. Donkers, L.C. Sögütoglu, H.P. Huinink, H.R. Fischer, O.C.G. Adan, A review of salt hydrates for seasonal heat storage in domestic applications, Appl. Energy 199 (2017) 45–68.
[12] J. Lizana, R. Chacartegui, A. Barrios-Padura, J.M. Valverde, Advances in thermal energy storage materials and their applications towards zero energy buildings: a critical review, Appl. Energy 203 (2017) 219–239.
[13] H.U. Rammelberg, T. Osterland, B. Priehs, O. Opel, W.K.L. Ruck, Thermochemical heat storage materials – performance of mixed salt hydrates, Sol. Energy 136 (2016) 571–589.
[14] I. Glaznev, I. Ponomarenko, S. Kirik, Y. Aristov, Composites $CaCl_2$/SBA-15 for adsorptive transformation of low temperature heat: pore size effect, Int. J. Refrig. 34 (5) (2011) 1244–1250.
[15] G.T. Whiting, D. Grondin, D. Stosic, S. Bennici, A. Auroux, Zeolite–$MgCl_2$ composites as potential long-term heat storage materials: influence of zeolite properties on heats of water sorption, Sol. Energy Mater. Sol. Cell. 128 (2014) 289–295.
[16] A. Permyakova, S. Wang, E. Courbon, F. Nouar, N. Heymans, P. d'Ans, N. Barrier, P. Billemont, G. De Weireld, N. Steunou, Design of salt–metal organic framework composites for seasonal heat storage applications, J. Mater. Chem. A 5 (25) (2017) 12889–12898.
[17] X. Zheng, T.S. Ge, R.Z. Wang, L.M. Hu, Performance study of composite silica gels with different pore sizes and different impregnating hygroscopic salts, Chem. Eng. Sci. 120 (2014) 1–9.
[18] X. Liu, H. Wang, X. Liu, F. Yang, L. Guan, S. Sani, C. Sun, Y. Wu, Development of $MgSO_4$/mesoporous silica composites for thermochemical energy storage: the role of porous structure on water adsorption, Energy Rep. 8 (2022) 4913–4921.
[19] L. Calabrese, D. Palamara, E. Piperopoulos, E. Mastronardo, C. Milone, E. Proverbio, Deviceful LiCl salt hydrate confinement into a macroporous silicone foam for low-temperature heat storage application, J. Sci.: Adv. Mater. Devices 7 (3) (2022) 100463.
[20] V. Brancato, L. Calabrese, V. Palomba, A. Frazzica, M. Fullana-Puig, A. Solé, L. F. Cabeza, $MgSO_4{\cdot}7H_2O$ filled macro cellular foams: an innovative composite sorbent for thermo-chemical energy storage applications for solar buildings, Sol. Energy 173 (2018) 1278–1286.
[21] J.X. Xu, T.X. Li, J.W. Chao, T.S. Yan, R.Z. Wang, High energy-density multi-form thermochemical energy storage based on multi-step sorption processes, Energy 185 (2019) 1131–1142.
[22] S.-Y. Li, Y.-J. Huo, T. Yan, H. Zhang, L.-W. Wang, W.-G. Pan, Preparation and thermal properties of zeolite/$MgSO_4$ composite sorption material for heat storage, Renew. Energy 224 (2024) 120166.
[23] D. Mahon, G. Claudio, P.C. Eames, An experimental investigation to assess the potential of using $MgSO_4$ impregnation and Mg^{2+} ion exchange to enhance the performance of 13X molecular sieves for interseasonal domestic thermochemical energy storage, Energy Convers. Manag. 150 (2017) 870–877.
[24] H. Zhang, S. Liu, A. Shukla, Y. Zou, X. Han, Y. Shen, L. Yang, P. Zhang, K. Kusakana, Thermal performance study of thermochemical reactor using net-packed method, Renew. Energy 182 (2022) 483–493.
[25] S. Xu, R. Wang, L. Wang, J. Zhu, A zeolite 13X/magnesium sulfate–water sorption thermal energy storage device for domestic heating, Energy Convers. Manag. 171 (2018) 98–109.
[26] D. Mahon, P. Henshall, G. Claudio, P.C. Eames, Feasibility study of $MgSO_4$ + zeolite based composite thermochemical energy stores charged by vacuum flat plate solar thermal collectors for seasonal thermal energy storage, Renew. Energy 145 (2020) 1799–1807.
[27] H.A. Ousaleh, S. Sair, S. Mansouri, Y. Abboud, M. Zahouily, A. Faik, A.E. Bouari, Enhanced inorganic salts stability using bentonite clay for high-performance and low-cost thermochemical energy storage, J. Energy Storage 49 (2022) 104140.
[28] V. Brancato, L.G. Gordeeva, A. Sapienza, V. Palomba, S. Vasta, A.D. Grekova, A. Frazzica, Y.I. Aristov, Experimental characterization of the LiCl/vermiculite composite for sorption heat storage applications, Int. J. Refrig. 105 (2019) 92–100.
[29] Q. Touloumet, G. Postole, L. Massin, C. Lorentz, A. Auroux, Investigation of the impact of zeolite shaping and salt deposition on the characteristics and performance of composite thermochemical heat storage systems, J. Mater. Chem. A 11 (6) (2023) 2737–2753.
[30] Q. Miao, Y. Zhang, X. Jia, Z. Li, L. Tan, Y. Ding, $MgSO_4$-expanded graphite composites for mass and heat transfer enhancement of thermochemical energy storage, Sol. Energy 220 (2021) 432–439.
[31] M. Gaeini, A.L. Rouws, J.W.O. Salari, H.A. Zondag, C.C.M. Rindt, Characterization of microencapsulated and impregnated porous host materials based on calcium chloride for thermochemical energy storage, Appl. Energy 212 (2018) 1165–1177.
[32] K. Posern, C. Kaps, Calorimetric studies of thermochemical heat storage materials based on mixtures of $MgSO_4$ and $MgCl_2$, Thermochim. Acta 502 (1–2) (2010) 73–76.
[33] M. Zbair, M.H. Nguyen, P. Dutournié, S. Bennici, Bi-salts composites to enhance the hydration kinetics and heat storage capacity, J. Energy Storage 73 (2023) 108862.
[34] A. Solé, L. Miró, C. Barreneche, I. Martorell, L.F. Cabeza, Corrosion of metals and salt hydrates used for thermochemical energy storage, Renew. Energy 75 (2015) 519–523.

[35] H.A. Ousaleh, S. Sair, S. Mansouri, Y. Abboud, A. Faik, A.E. Bouari, New hybrid graphene/inorganic salt composites for thermochemical energy storage: synthesis, cyclability investigation and heat exchanger metal corrosion protection performance, Sol. Energy Mater. Sol. Cell. 215 (2020) 110601.
[36] Z. Wang, X.K. Xu, T. Yan, H. Zhang, L.W. Wang, W.G. Pan, Preparation and thermal properties of zeolite 13X/$MgSO_4$-LiCl binary-salt composite material for sorption heat storage, Appl. Therm. Eng. 245 (2024) 122905.
[37] Z. Chen, Y. Zhang, Y. Zhang, Y. Su, S. Riffat, A study on vermiculite-based salt mixture composite materials for low-grade thermochemical adsorption heat storage, Energy 278 (2023) 127986.
[38] W. Li, M. Zeng, Q. Wang, Development and performance investigation of $MgSO_4$/$SrCl_2$ composite salt hydrate for mid-low temperature thermochemical heat storage, Sol. Energy Mater. Sol. Cell. 210 (2020) 110509.
[39] Y. Zhang, Z. Chen, C. Kutlu, Y. Su, S. Riffat, Investigation on a vermiculite-based solar thermochemical heat storage system for building applications, Future Cities Environ. 8 (1) (2022) 8.
[40] A.R. Khan, M. Khan, A.U. Rehman, T.Y. Zhao, M. Zheng, Novel synthesis and structural investigations of $ZnSO_4$/$MgCl_2$ composite hydrated salt for enhanced thermochemical heat storage applications, Russ. J. Inorg. Chem. 67 (7) (2022) 1125–1134.
[41] A.U. Rehman, M. Khan, Z. Maosheng, Hydration behavior of $MgSO_4$–$ZnSO_4$ composites for long-term thermochemical heat storage application, J. Energy Storage 26 (2019) 101026.
[42] W. Ji, H. Zhang, S. Liu, Z. Wang, S. Deng, An experimental study on the binary hydrated salt composite zeolite for improving thermochemical energy storage performance, Renew. Energy 194 (2022) 1163–1173.
[43] K. Korhammer, M.-M. Druske, A. Fopah-Lele, H.U. Rammelberg, N. Wegscheider, O. Opel, T. Osterland, W. Ruck, Sorption and thermal characterization of composite materials based on chlorides for thermal energy storage, Appl. Energy 162 (2016) 1462–1472.
[44] H. Zhao, Z. Wang, Q. Li, T. Wu, M. Zhang, Q. Shi, Water sorption on composite material "zeolite 13X modified by LiCl and $CaCl_2$", Microporous Mesoporous Mater. 299 (2020) 110109.
[45] S.P. Casey, D. Aydin, J. Elvins, S. Riffat, Salt impregnated desiccant matrices for 'open' thermochemical energy conversion and storage – improving energy density utilisation through hygrodynamic & thermodynamic reactor design, Energy Convers. Manag. 142 (2017) 426–440.
[46] A.A. Hawwash, H. Hassan, K.E. feky, Impact of reactor design on the thermal energy storage of thermochemical materials, Appl. Therm. Eng. 168 (2020) 114776.
[47] J. Rui, Y. Luo, M. Wang, J. Peng, X. She, Design and performance evaluation of an innovative salt hydrates-based reactor for thermochemical energy storage, J. Energy Storage 55 (2022) 105799.
[48] R.J. Sutton, E. Jewell, J. Elvins, J.R. Searle, P. Jones, Characterising the discharge cycle of $CaCl_2$ and $LiNO_3$ hydrated salts within a vermiculite composite scaffold for thermochemical storage, Energy Build. 162 (2018) 109–120.
[49] C. Strong, Y. Carrier, F. Handan Tezel, Experimental optimization of operating conditions for an open bulk-scale silica gel/water vapour adsorption energy storage system, Appl. Energy 312 (2022) 118533.
[50] K. Walayat, J. Duesmann, T. Derks, A.h. Mahmoudi, R. Cuypers, M. Shahi, Experimental and numerical investigations for effective thermal conductivity in packed beds of thermochemical energy storage materials, Appl. Therm. Eng. 193 (2021) 117006.
[51] W. Li, J.J. Klemeš, Q. Wang, M. Zeng, Salt hydrate–based gas-solid thermochemical energy storage: current progress, challenges, and perspectives, Renew. Sustain. Energy Rev. 154 (2022) 111846.
[52] D.A. Bardy, C.A. Cruickshank, F.H. Tezel, Y.H. Carrier, B. Wong, An experimental investigation of fixed and fluidized beds as adsorbers in compact thermal energy storage systems, J. Energy Storage 31 (2020) 101648.
[53] L.F. Marie, T.S. O'Donovan, Fluidisation of thermochemical energy storage materials: degradation assessment, Energy Sources, Part A Recovery, Util. Environ. Eff. 45 (4) (2023) 10034–10050.
[54] J. Zhu, C. Gao, F. Kong, K. Zhang, Z. Bai, J. Guo, Low-priced stable $SrCl_2$@SG composite sorbents for low-grade solar heat storage application in open sorption systems, Sol. Energy Mater. Sol. Cell. 229 (2021) 111118.
[55] H. Yang, C. Wang, L. Tong, S. Yin, L. Wang, Y. Ding, Salt hydrate adsorption material-based thermochemical energy storage for space heating application: a review, Energies 16 (6) (2023) 2875.
[56] A. Palacios, M.E. Navarro, C. Barreneche, Y. Ding, Water sorption-based thermochemical storage materials: a review from material candidates to manufacturing routes, Fronti. Thermal Eng. 2 (2022) 1003863.
[57] H. Wang, X. Liu, X. Liu, C. Sun, Y. Wu, Fluidizable mesoporous silica composites for thermochemical energy storage, Energy (2023) 127255.
[58] X. Liu, X. Liu, F. Yang, Y. Wu, Experimental investigation of low-temperature fluidised bed thermochemical energy storage with salt-mesoporous silica composite materials, Appl. Energy 362 (2024) 122953.
[59] D. Geldart, Types of gas fluidization, Powder Technol. 7 (5) (1973) 285–292.
[60] J.A. Almendros-Ibáñez, M. Fernández-Torrijos, M. Díaz-Heras, J.F. Belmonte, C. Sobrino, A review of solar thermal energy storage in beds of particles: packed and fluidized beds, Sol. Energy 192 (2019) 193–237.
[61] F. Raganati, R. Chirone, P. Ammendola, Calcium-looping for thermochemical energy storage in concentrating solar power applications: evaluation of the effect of acoustic perturbation on the fluidized bed carbonation, Chem. Eng. J. 392 (2020) 123658.
[62] J. Lin, Q. Zhao, H. Huang, H. Mao, Y. Liu, Y. Xiao, Applications of low-temperature thermochemical energy storage systems for salt hydrates based on material classification: a review, Sol. Energy 214 (2021) 149–178.
[63] K. Posern, C. Kaps, Humidity controlled calorimetric investigation of the hydration of $MgSO_4$ hydrates, J. Therm. Anal. Calorim. 92 (3) (2008) 905–909.
[64] P.A. Kallenberger, K. Posern, K. Linnow, F.J. Brieler, M. Steiger, M. Fröba, Alginate-derived salt/polymer composites for thermochemical heat storage, Adv. Sustain. Sys. 2 (7) (2018).
[65] E. Courbon, P. D'Ans, A. Permyakova, O. Skrylnyk, N. Steunou, M. Degrez, M. Frère, Further improvement of the synthesis of silica gel and $CaCl_2$ composites: enhancement of energy storage density and stability over cycles for solar heat storage coupled with space heating applications, Sol. Energy 157 (2017) 532–541.
[66] A.I. Shkatulov, J. Houben, H. Fischer, H.P. Huinink, Stabilization of K_2CO_3 in vermiculite for thermochemical energy storage, Renew. Energy 150 (2020) 990–1000.
[67] C. Peng, L. Chen, M. Tang, A database for deliquescence and efflorescence relative humidities of compounds with atmospheric relevance, Fundamental Res. 2 (4) (2022) 578–587.
[68] E. Bérut, L. Bois, Q. Touloumet, J. Outin, M. Ondarts, G. Postole, M.J.R. López, A. Auroux, N.L. Pierrès, Characterization of silica-PEG-$CaCl_2$ composite sorbents in an open thermochemical heat storage reactor, J. Energy Storage 72 (2023) 108632.
[69] S. Shervani, C. Strong, F.H. Tezel, Simultaneous impregnation and microencapsulation of $CaCl_2$ using silica gel and methyl cellulose for thermal energy storage applications, Sci. Rep. 14 (1) (2024) 7183.